Journal Pre-proof

Efficient green-emitting Tb^{3+}-doped di-ureasil coating phosphors for near-UV excited light-emitting diodes

Ming Fang, Airton G. Bispo-Jr, Lianshe Fu, Rute A.S. Ferreira, Luís D. Carlos

PII: S0022-2313(19)32039-3

DOI: https://doi.org/10.1016/j.jlumin.2019.116910

Reference: LUMIN 116910

To appear in: *Journal of Luminescence*

Received Date: 17 October 2019

Revised Date: 5 November 2019

Accepted Date: 21 November 2019

Please cite this article as: M. Fang, A.G. Bispo-Jr, L. Fu, R.A.S. Ferreira, Luí.D. Carlos, Efficient green-emitting Tb^{3+}-doped di-ureasil coating phosphors for near-UV excited light-emitting diodes, *Journal of Luminescence* (2019), doi: https://doi.org/10.1016/j.jlumin.2019.116910.

Efficient green-emitting Tb^{3+}-doped di-ureasil coating phosphors for near-UV excited light-emitting diodes

Ming Fang [a], Airton G. Bispo-Jr [a,b], Lianshe Fu [a], Rute A. S. Ferreira [a,*], Luís D. Carlos [a,*]

[a] *Department of Physics, CICECO–Aveiro Institute of Materials, University of Aveiro, 3810-193 Aveiro, Portugal*

[b] *São Paulo State University (UNESP), School of Technology and Sciences, Presidente Prudente, SP, 19060-900, Brazil and UNESP-Institute of Biosciences, Humanities and Exact Sciences, São José do Rio Preto, SP, 15054-000, Brazil*

Keywords: Light-emitting diode; Terbium; Green color; Di-ureasil; Photoluminescence; Solid-state lighting

*Corresponding author. Department of Physics, CICECO–Aveiro Institute of Materials, University of Aveiro, 3810-193 Aveiro, Portugal.

Email address: rferreira@ua.pt (Rute A. S. Ferreira) and lcarlos@ua.pt (Luís D. Carlos).

ABSTRACT

Light-emitting diodes (LEDs) are replacing conventional lighting sources, like incandescent and fluorescent lamps, due to their higher efficiency, lower energy consumption and environmental friendliness characteristics. Additional applications envisaging “engineered light” able to control the human circadian rhythm are now in place with emphases on green-emitting LEDs. In this work, transparent and flexible coatings based on organic–inorganic di-ureasil hybrids doped in-situ with a terbium (Tb^{3+}) complex involving salicylic acid as ligands were synthesized. The materials are transparent, essentially amorphous and thermal stable up to 180 °C. Under near-UV excitation, bright green emission with high quantum yield (0.565±0.057) and enhanced photostability are observed. Green-emitting prototypes were fabricated using a commercial near-UV-emitting LED (NUV-LED) combined with the Tb^{3+}-doped di-ureasil coating showing narrow-band green emission with yellowish-green color coordinates (Commission Internationale de l'Éclairage, CIE 1931) of (0.329, 0.606) and high luminous efficacy (21.5 lm/W). This efficacy is the largest one reported for analogous prototypes formed by an NUV-LED coated with a green-emitting phosphor prepared under mild synthetic conditions (<100 °C), demonstrating that in-situ formation of carboxylate lanthanide-based complexes is an energy saving process with potential for solid-state lighting and backlight for flexible displays.

1. Introduction

Lighting as one of the indispensable human technologies has been widely applied to human activities, including basic illumination and decoration [1]. Light-emitting diodes (LEDs) emerged in the last decades as an efficient solid-state lighting source not only replacing the traditional incandescent and compact fluorescent light bulbs [2], but also featuring more uncommon applications in the fields of human health and productivity due to their "engineered light" able to control the circadian rhythm [3–5]. LEDs, however, still face some shortcomings such as an insufficient cyan emission limiting color render index and a relatively low efficient green emission, termed as "cyan gap" and "green gap" problems, respectively [6,7]. Monochromatic green-emitting devices are particularly desirable due to the larger sensibility of the human eyes in this spectral region [8], pushing, therefore, solid-state lighting to pay particular attention to the development of green-emitting LEDs. Contrarily to what found for LEDs with emission the blue or red spectral regions, the development of green-emitting devices has been limited so far due to the "green gaps" [7]. While fabricating for red- and blue-emitting LEDs high luminous efficacy (LE) is attained simply by adjusting the relative amount of indium in InGaN or AlInGaP, for the green-emitting ones, this methodology induces a decrease in the LE [9]. An alternative approach to overcome the "green gap" is the combination of near-UV emitting LEDs (NUV-LEDs) and down-shifting phosphors able to efficiently convert the near-UV radiation from GaN-based LEDs into green light [10].

Complexation of lanthanide ions (Ln^{3+}) with organic ligands has been extensively applied to develop efficient phosphors for LED applications, given the intrinsic pure and tunable emission colors of the ions. The judicious choice of the ligands requires high-absorption coefficients in the UV spectral region and efficient intramolecular energy transfer to the Ln^{3+}

excited states [11]. For sensitizing the Ln^{3+} ions, whereas *β*-diketonates and carboxylates are frequently used as the primary ligands, heterocyclic moieties are used as ancillary ones [12]. Compared to Ln^{3+}-based complexes involving *β*-diketonate ligands, carboxylate complexes usually show improved photo- and thermal-stabilities due to their polymeric nature [13]. As a result, Ln^{3+}-based complexes with carboxylates could be regarded as prospective phosphors for lighting and display applications. In particular, aromatic carboxylic acids typically have strong absorption in the UV or near-UV spectral regions due to the delocalized π-electron system of aromatic rings and have been widely used to prepare Ln^{3+}-based coordination polymers [14–24]. Among those complexes, examples involving hydroxybenzoic acids, especially salicylic acid (HSal) and their derivatives, already displayed promising luminescence features [21–24]. In what concerns processability, these complexes should be incorporated into solid-state matrices enabling easy film fabrication, which is a relevant property featuring the use of UV-LED. Nonetheless, the polymeric characteristic of the complexes with short-range interactions [25], renders them with poor solubility in common organic solvents, preventing their direct incorporation in matrices.

Up to now, those complexes were incorporated into aminoclays [26] and organic–inorganic hosts either via covalent binding or physical embedding by in-situ sol–gel process [27–30]. Focusing our attention on Tb^{3+}-derived complexes due to the intrinsic green color, mention must be done to examples involving HSal and 1,10-phenanthroline (phen) ligands doped into polyvinyl alcohol (PVA) [31]. Although some of the Tb^{3+}-derived complexes with aromatic carboxylates display high emission quantum yields (~0.50), the maximum excitation wavelength lies in the UV region (~320 nm), which is not suitable for excitation with NUV-LED chips (>350 nm) [15,21,32]. Therefore, the design and synthesis of new near-UV excited

phosphors are critical issues. Few works reported the sensitization of Tb^{3+}-related luminescence by aromatic carboxylate ligands in the near-UV region [33–36]. For instance, the Tb^{3+}-based macrocyclic complex with pyrazoyl-1-azaxanthone shows the maximum excitation wavelength at 355 nm [33], while the complex bearing the 2-hydroxyisophthalate moiety displays the strongest excitation wavelength at 370 nm [34]. The $Tb_9(Hesa)_{16}(\mu\text{-}OH)_{10}(NO_3)$ (Hesa=hexyl salicylate) hydroxo cluster exhibits a red-shift of the absorption band from 315 to 340 nm, due to phenyl stacking [35]. The Tb^{3+}-based complex with 4-benzoylbenzoic acid and undecylenic acid, as primary and reactive ligands, respectively, is characterized by a wide excitation range (310–400 nm) [36]. It should be noted that an intriguing work was reported showing that using HSal as primary ligand and trioctylphosphine oxide as a neutral ligand the obtained Tb^{3+}-based complex can render soluble even in non-polar matrices [32].

Inspired by the aforementioned works, and aiming at synthesizing green phosphors with high quantum yields under near-UV excitation, herein we incorporate high doping concentrations of a Tb^{3+}-based complex involving the HSal ligand into organic–inorganic di-ureasil hybrids by in-situ sol–gel method, overcoming solubility issues, as di-ureasils have unique polymeric structures with different coordination points that can interact with the Tb^{3+} ions [37]. The resulting luminescent di-ureasils were structurally and spectrally characterized, displaying a photostable and bright green emission (quantum yield of 0.565±0.057). Green-emitting LEDs prototypes were also fabricated using commercial available NUV-LEDs (365 nm) combined with the Tb^{3+}-doped di-ureasil coating showing the largest LE (21.5 lm/W) reported so far for analogous prototypes formed by an NUV-LED coated with a green-emitting phosphor prepared under mild synthetic conditions (<100 °C).

2. Experimental section

2.1. Chemical and materials

Sodium salicylate (NaSal, Acofarma, 99%), HSal (Acofarma, Madrid, Spain), α,ω-diaminepoly(oxyethylene-co-oxypropylene) (ED-600, Huntsman), and 3-isocyanateproplytriethoxysilane (ICPTES, 95%, Aldrich) are commercially available. A terbium chloride ($TbCl_3$) aqueous solution (0.1 mol/L) was obtained by dissolving terbium oxide (Tb_4O_7, Yuelong New Material Co., Ltd., Shanghai, China) in hydrochloride acid (HCl, 37%, Aldrich). The remaining acid was removed by successive evaporation and the resulting solid was dissolved in distilled water. Tetrahydrofuran (THF, 99%, Sigma–Aldrich) and absolute ethanol (EtOH, Sigma–Aldrich) were used as solvents. The HCl and sodium hydroxide (NaOH, AkzoNobel, Barcelona, Spain) were used for the formation of gels. All chemicals were used as received without purifications. Distilled water was used throughout experiments. The commercial NUV-LED chips (365±5 nm) were purchased from Shenzhen Looking Long Technology Co., Ltd., Shenzhen, China.

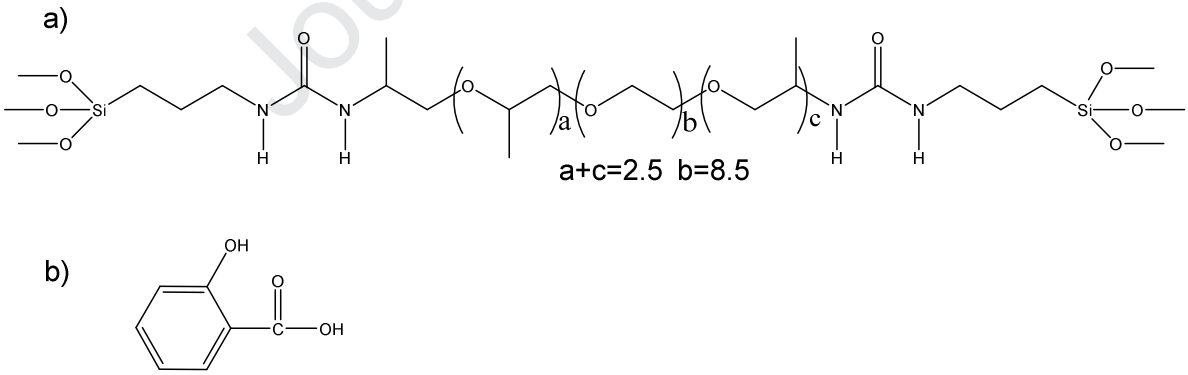

Scheme 1. Molecular structures of (a) dU(600) and (b) HSal ligand.

2.2. Synthesis of d-UPTES(600) precursor

The non-hydrolised precursor, d-UPTES(600), used for the preparation of the di-ureasil, dU(600), was synthesized according to the literature [38]. The ICPTES was added dropwise into a homogenous mixture of ED-600 and THF under stirring at room temperature with the molar ratio of ED-600:ICPTES=1:2. After 24 h of stirring at room temperature, the THF in the mixture was evaporated under vacuum, and the d-UPTES(600) precursor was achieved.

2.3. Synthesis of dU(600) doped in-situ with a Tb^{3+}-based complex

For the preparation of the non-doped dU(600), 1.0 g (0.913 mmol) of d-UPTES(600) was mixed with 1 mL of EtOH and 98.6×10^{-6} L of HCl (0.05 mol/L) in a beaker for 30 minutes stirring. The mixture was then transferred into an oven at 50 ^{o}C. The molecular structure of the dU(600) is illustrated in Scheme 1. For the preparation of the dU(600)-based hybrids containing distinct concentrations of the Tb^{3+} complex with HSal, 1.0 g (0.913 mmol) of d-UPTES(600) was mixed with 1 mL of EtOH in three isolated beakers. Then 98.6×10^{-6} L of HCl (0.05 mol/L) was added with a molar ratio of d-UPTES(600):H_2O=1:6 to the three isolated beakers. The resulting sols were stirred at room temperature for 30 minutes. Simultaneously, 9.13×10^{-4}, 1.826×10^{-3} and 2.739×10^{-3} L of $TbCl_3$ (0.1 mol/L) aqueous solutions were added to another three separated beakers and dried at 95 ^{o}C to evaporate the water. Then, they were dissolved in 4×10^{-3} L of EtOH, followed by addition of 37.9×10^{-3}, 75.7×10^{-3} and 113.6×10^{-3} g of HSal (Scheme 1) with a molar ratio of dU(600):Tb:HSal=1:c:3c (c=10%, 20% and 30%), respectively. These mixtures were added to the above sols, separately, followed by 10 minutes of stirring at room temperature. Finally, 54.8×10^{-6}, 110.0×10^{-6}, and 164.5×10^{-6} L of NaOH (5.0 mol/L) were added to the above mentioned three sols under stirring, with a molar ratio of HSal:NaOH=1:1. The resulting transparent sols were transferred to a model and placed in an oven of 50 ^{o}C for two days. The samples with doping concentrations of 10%, 20% and 30% are designated as

10TbSal@dU6, 20TbSal@dU6, and 30TbSal@dU6, respectively. The Tb content in the final hybrids was determined by Inductively Coupled Plasma Optical Emission Spectroscopy (ICP-OES) as 1.3±0.1, 2.5±0.3, and 3.9±0.4 wt%, for 10TbSal@dU6, 20TbSal@dU6, and 30TbSal@dU6 respectively. These values are in accord with the calculated ones, 1.7±0.2, 3.2±0.3 and 4.6±0.4 wt%, respectively, being the minor deviations assigned to residual solvent and the unfinished condensation reaction. The uniform distribution of the complex within the hybrid is inferred from scanning electronic microscopy (SEM) images and energy-dispersive X-ray spectroscopy (EDX) elemental maps of 30TbSal@dU6 that reveal a smooth surface and a homogenous distribution of the Si and Tb atoms, without evidence of aggregation, (Fig. S1). We note that at higher dopant molar ratios (e.g., 40 mol%) transparency is lost. Fig. 1a and 1b display photographs of a transparent 30TbSal@dU6 thick film under day light and 365 nm illumination, respectively.

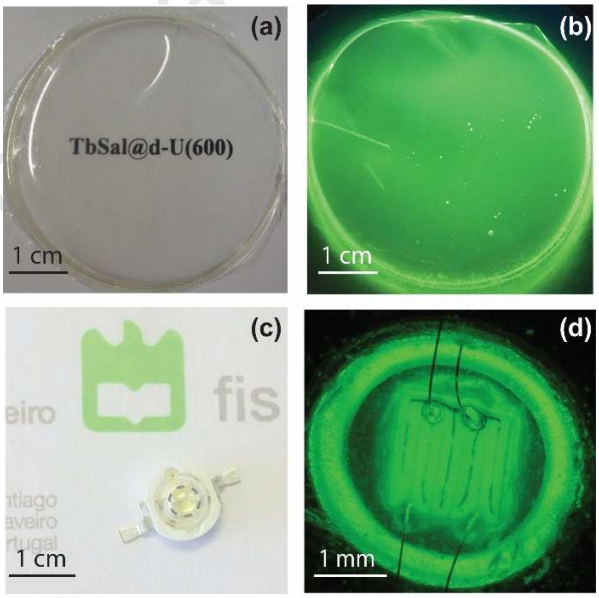

Fig. 1. Photographs of a free standing film of 30TbSal@dU6 under (a) day light and (b) near-UV radiation (365 nm); In (c) a commercial NUV-LED chips (365 nm) coated with 30TbSal@dU6 is

shown (the grey dashed circle signs the hybrid coating), whereas the photo in (d) zooms the LED operating at 5.0×10^{-3} A of driving current.

2.4. Synthesis of the Tb^{3+} complex

The pure Tb^{3+}-based complex with HSal ligand, $Tb(Sal)_3{\cdot}H_2O$, designated as Tb-I, was synthesized according to the literature [39].

2.5. Prototypes of green-emitting LEDs fabrication

The green-emitting LEDs prototypes were fabricated as followed: a droplet (1.0×10^{-5} L) of the 30TbSal@dU6 sol was drop-casted on the surface of a commercial NUV-LED. Then, the LED was moved into an oven (50 ^{o}C) for 2 days for complete gelification and solvent removal. To ensure reproducibility, three prototypes were made, under the same experimental conditions. Fig. 1c shows a photograph of the as-fabricated prototype under daylight and the zoomed photo in Fig. 1d displays the same LED upon 5×10^{-3} A of driving current.

2.6. Measurements

UV−visible absorption spectra were measured using a dual-beam spectrometer Lambda 950 (PerkinElmer) at a resolution of 1.0 nm. Powder X-ray diffraction (XRD) patterns were recorded in the 2θ range of 3.5 to 60.0° by using Panalytical Empyrean Diffractometer under exposure of CuK_{α} radiation (1.54 Å). Fourier transform infrared (FT-IR) spectra from 4000 to 400 cm^{-1} with 64 scans and 4 cm^{-1} resolution were obtained by using MATTSON 7000 FT-IR Spectrometer. The best fit of the experimental data was sought by varying the frequency, bandwidth, and intensity of the bands and by employing Lorentzian/Gaussian contributions. FT-Raman spectra were obtained at room temperature with a Bruker RFS 100/S spectrometer equipped with a Nd:YAG laser (1064 nm, 350 mW). The Raman intensities were collected over the 4000–50 cm^{-1} range at a resolution of 4 cm^{-1}. Thermogravimetric (TG) measurements were

performed with a 10 ^{o}C/min heating speed under the air atmosphere on an SDT 2960 analyzer (Shimadzu, Japan). The Tb content was determined by ICP-OES (Inductively Coupled Plasma Optical Emission Spectroscopy) analysis on a Horbia-Jobin Yvon model Activa-M. SEM analyses were carried out using a scanning electron microscope Hitachi SU-70 operating at an accelerating voltage of 15 kV and an EDX from Bruker. Excitation and emission spectra were recorded using a Fluorolog3® Horiba Scientific spectroscope (Model FL3-2T) with a modular double grating excitation spectrometer and a TRIAX 320 single emission monochromator, coupled to an R928 Hamamatsu photomultiplier using the front face acquisition mode. A 450 W Xe arc lamp was used as the excitation source. The emission spectra were corrected for the detection and optical spectral response of the spectrofluorimeter and the excitation spectra were corrected for the spectral distribution of the lamp intensity using a photodiode reference detector. The emission decay curves were measured with the setup described for the luminescence spectra using a pulsed Xe−Hg lamp (6 μs pulse at half-width and 20−30 μs tail). The absolute emission quantum yields (*q*) were measured at room temperature using the C13534 system from Hamamatsu with a 150 W xenon lamp coupled to a monochromator for wavelength discrimination, an integrating sphere as sample chamber and two multichannel analyzers for signal detection. Three measurements were made for each sample and the average value with an accuracy of 10% is reported. The radiant flux (W) and the luminous flux (lm) of the prototypes (coated NUV-LED) were measured using an integrating sphere ISP 150L-131 from Instrument Systems. The integrating sphere ($BaSO_4$ coating) has an internal diameter of 150 mm and was coupled to an array spectrometer MAS 40 from Instrument Systems. The measurements are accurate within 5%, accordingly to the manufacturer. The phosphor performance was evaluated under continuous excitation at 365 nm (450 W, Xe arc lamp, 3.5×10^{-3} W irradiation).

3. Results and discussion

3.1. Structural studies

The powder XRD patterns of 10TbSal@dU6, 20TbSal@dU6, and 30TbSal@dU6 are given in Fig. S2. All the patterns show a broad band centred at *ca.* 21.0° ascribed to the presence of amorphous siliceous domains from the dU(600) host [40]. The second-order of this peak appears as a very broad weak hump around 35.0–50.0°. Accordingly, the structural unit distances are estimated, using the Bragg law [41], to be 4.3±0.1, 4.2±0.1 and 4.2±0.1 Å for 10TbSal@dU6, 20TbSal@dU6, and 30TbSal@dU6, respectively, resembling that previously reported (4.2±0.1 Å) for dU(600) [42]. The sharp peaks at 31.9, 45.6, and 56.6° result from the diffraction of NaCl (Fig. S2), that was formed when Cl^- ions in $TbCl_3$ react with Na^+ ions in NaOH.

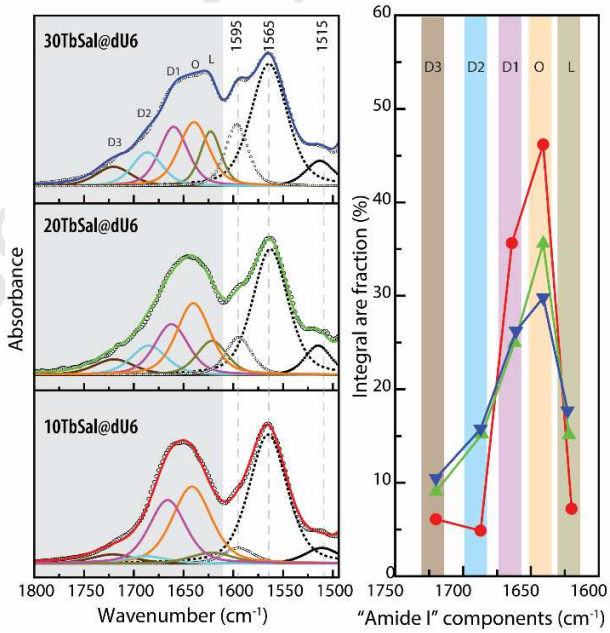

Fig. 2. (a) Curve-fitting results of the FT-IR "Amide I" region of 10TbSal@dU6 (red line), 20TbSal@dU6 (green line) and 30TbSal@dU6 (blue line); (b) Integral area fraction of the

resolved components of the "Amide I" bands of 10TbSal@dU6 (red line/symbol), 20TbSal@dU6 (green line/symbol) and 30TbSal@dU6 (blue line/symbol).

The local structure of 10TbSal@dU6, 20TbSal@dU6, 30TbSal@dU6 were further investigated by FT-IR (Fig. S3**)**. The disappearance of the strong band at 2272 cm^{-1} related to the isocyanate moiety of ICPTES in all the spectra indicates that the functional amine groups fully react with ICPTES (Fig. S3). Looking for evidence of the Tb^{3+} local coordination in the hybrid host through the oxygen atom of the carbonyl group of the urea cross-linkages, we inspect the ''Amide I'' and ''Amide II'' regions (1800–1490 cm^{-1}) [43], in Fig. 2a. For dU(600), in "Amide I" region, the three individual components centred at ~1720 (**D3**), 1686 (**D2**), and 1662 (**D1**) cm^{-1} are assigned to the absorptions of hydrogen-bonded C=O groups of disordered poly-(oxyethylene) (POE)/urea aggregates of increasing strength, whereas the prominent band appeared at around 1640 cm^{-1} (**O**) is due to the absorption of C=O groups included in significantly more ordered hydrogen-bonded urea–urea aggregates [44]. Typically, the coordination of Ln^{3+} ions to the C=O oxygen atoms of the urea cross-linkages of the di-ureasil matrix is easily discerned in the "Amide I" region through the detection of a new event around 1620 cm^{-1} (**L**) [44,45]. The results of the curve-fitting performed in the "Amide I" and "Amide II" bands of 10TbSal@dU6, 20TbSal@dU6, and 30TbSal@dU6 (Fig. 2a) and the integral area fraction of the resolved components of "Amide I" (Fig. 2b, and Table S1 for the relative component percentages) fully supports the interaction between Tb^{3+} ions and the C=O groups of the urea bridges. Indeed, increasing the Tb^{3+} amount the intensities of the 1662 and 1640 cm^{-1} components are reduced, while that of the 1620 cm^{-1} increases significantly. These findings are indicative of the disruption of urea–urea aggregates **O** and strongest POE/urea aggregates **D1**, respectively, with the concomitant formation of a Tb^{3+} coordination-sensitive feature and more

POE/urea aggregates **D2** (the intensity of the 1686 cm^{-1} component increases as the Tb^{3+} concentration increases). In the "Amide II" region, the low-relative intensity band at 1515 cm^{-1} is attributed to the presence of weaker hydrogen-bonded urea–urea structures [38], while that at 1595 cm^{-1} (that increases with the increasing of the Tb^{3+} concentration) is due to asymmetric –COO^{-} vibrations from Sal ligands [46,47].

The hybrids' local structure was further studied by FT-Raman spectroscopy, to ascertain the formation of the Tb^{3+}-based complex during in-situ synthesis process. To assist an easier interpretation of the data, the FT-Raman spectra of the dU(600) and the pure HSal, NaSal, and Tb-I are given out in Fig. S4. The FT-Raman spectra of the Tb^{3+}-based hybrids are composed of the components found for dU(600) and Tb-I, with no evidence of the NaSal and HSal contributions (Table S2), supporting, therefore, the formation of the Tb^{3+}-based complex by in-situ sol-gel process.

The thermal stabilities of the hybrids were also evaluated through the comparison among the TGA data of dU(600), Tb-I and 30TbSal@dU6 (Fig. S5). For Tb-I, the thermal decomposition process takes four steps. The first weight loss occurs from 150 to 180 °C due to the removal of one water molecule from the lattice (calcd.: 3.1%, found: around 3.5%). Further weight losses are attributed to the formation of the intermediate products $(1/2)Tb(C_6H_4OHCOO)_3\cdot(1/4)Tb_2O_2CO_3$ (calcd: 63.9%, found: around 66.5%) and $(1/3)Tb(C_6H_4OHCOO)_3\cdot(1/3)Tb_2O_2CO_3$ (calcd: 53.9%, found: around 48.9%), respectively [48]. The final weight loss is associated with the decomposing of residues and forming Tb_2O_3 (calcd: 31.1%, found: around 32.0%) [49]. This decomposition process of Tb-I is similar to the decomposition behavior of the binuclear terbium complex $[Tb_2(HSal)_8(H_2O)_2][(Hphen)_2]\cdot 2H_2O$ [50] that losses lattice and coordinated water molecules between 107 to 171 °C (observed,

3.65%; calculated, 3.89%). Moreover, the two chelating salicylate groups (observed, 36.18%, calculated, 34.43%.) decompose from 171 to 291 °C. For dU(600), the first weight losses before 100 °C is ascribed to the removal of the absorbed water and residual organic solvent. The main weight loss happened when the temperature is in the range of 175 to 327 °C, with around 53%, due to the decomposition of Jeffamine moieties, and the next weight change is related to the gradual loss of the remaining organic moieties and forming SiO_2 (calcd.: 13.7%, found: 14.4%) [51]. For the 30TbSal@dU6 hybrid, two significant weight losses due to the decomposition of polymer chains are discerned in the range of 180 to 630 °C [42]. Moreover, three extra weight losses (marked with arrows) are consistent with the decomposition behavior of Tb-I (except the weight loss of lattice water around 107 to 171 °C). This evidence hints that there is no water located on the first coordination shell of Tb^{3+} ions. For 30TbSal@dU6, the decomposition of Sal mainly occurs at around 287 °C, 383 °C, and 545 °C, with the final residual of SiO_2, NaCl and Tb_2O_3 (calcd.: 16.2%, found: 16.9%). The thermal decomposition of the in-situ synthesized Tb^{3+} complex is similar to that of pure Tb-I. In summary, the Tb^{3+}-based hybrids are stable up to 180 °C making them suitable for LED-based applications.

3.2. Optical properties

Fig. 3a displays the UV–visible absorption spectra of free-standing films of 10TbSal@dU6, 20TbSal@dU6, and 30TbSal@dU6, revealing that all are transparent. The spectra are dominated by a broadband in the region 250–325 nm that overlaps the absorption region of the undoped dU(600) hybrid [52], and the pure HSal located at 238 and 305 nm ($S_2 \leftarrow S_0$ and $S_1 \leftarrow S_0$ transitions, respectively) [53]. The maximum absorption wavelengths are ~348, ~350 and ~357 nm, for 10TbSal@dU6, 20TbSal@dU6, and 30TbSal@dU6, respectively,

with a red-shift tendency relying on the dopant amount, being observed a maximum absorption coefficient for the 20TbSal@dU6 (47 cm^{-1}, at 348 nm). However, around the near-UV region of interest for the use of commercial NUV LEDs (~365 nm), the 30TbSal@dU6 film displays the largest absorption coefficient (inset in Fig. 3a). The red-shift of the absorption onset as the Tb^{3+} concentration increases resembles that reported for the similar $Tb(Sal)_3(TOPO)_2$ (TOPO=trioctylphosphine oxide) complex [32], whose absorption (~350 nm) deviates as the dopants concentration increases (0.05–0.75 wt%). Such dependence was ascribed to the enhanced stack possibility of the aromatic rings caused by the increasing of organic dopants [16]. Increasing the dopant concentration enforces the interactions between the aromatic ligands and consequently forms more "π-stacking" which also results in the red-shift of excitation, consistent with the results of UV–visible spectra.

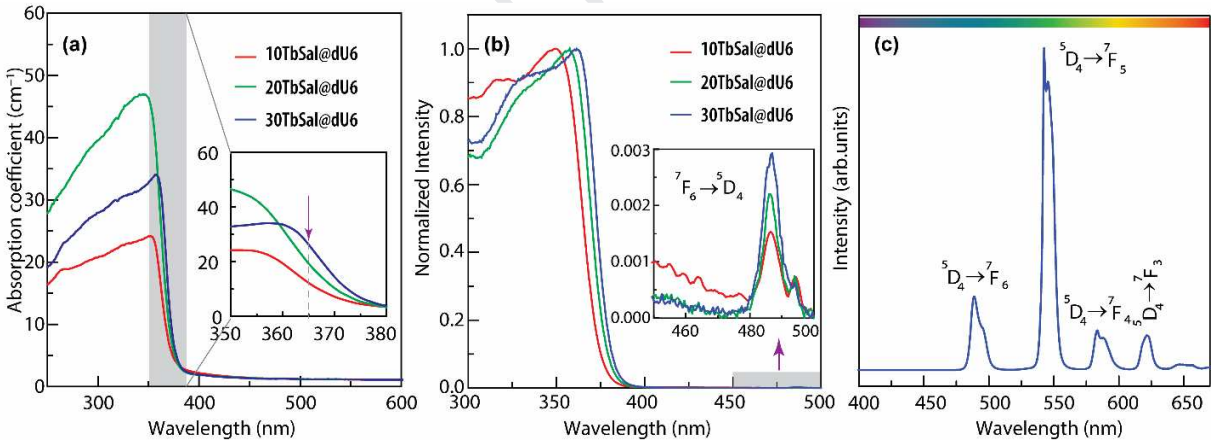

Fig. 3. (a) UV–visible absorption and (b) normalized excitation spectra (monitored at 543 nm of Tb^{3+} $^5D_4 \rightarrow {}^7F_5$ transitions) of 10TbSal@dU6, 20TbSal@dU6, and 30TbSal@dU6; (c) emission spectrum of 30TbSal@dU6 excited at 362 nm (maximum excitation wavelength).

The room temperature excitation and emission spectra of 10TbSal@dU6, 20TbSal@dU6, and 30TbSal@dU6 (Fig. 3b and Fig. S6a) are analogous and, thus, in Fig. 3c we show the

illustrative emission spectrum of 30TbSal@dU6. The excitation spectra resemble the absorption one, revealing a broadband in the UV region ascribed to the overlapped contribution of the dU(600) excited states and those from the ligands (Fig. 3b). The maximum excitation wavelength (~350, ~358 and ~362 nm, for 10TbSal@dU6, 20TbSal@dU6, and 30TbSal@dU6, respectively) shifts to the red as the dopant concentration increases. The spectra also reveal the low-relative intensity $^7F_6 \rightarrow {}^5D_4$ intra-4f^8 transition pointing out that the ligands dominate the Tb^{3+} sensitization, enabling the excitation of the hybrids with commercial NUV-LEDs. Moreover, the resonance between the triplet energy level of Sal (24184 cm^{-1}) and of the Tb^{3+} $^5D_4$ level (20500 cm^{-1}) [54,55] (an energy gap of 3684 cm^{-1}) favours efficient ligand-to-metal energy transfer [56].

The emission spectra are governed by the typical intra-4f^8 $^5D_4 \rightarrow {}^7F_{6-3}$ emission lines (Fig. 3c). The higher relative intensity and low FWHM (<10 nm) of the $^5D_4 \rightarrow {}^7F_6$ transition in the green spectral range (~545 nm) confers superior color purity [57,58], and larger overlap with the maximum spectral sensitivity of the human eye (555 nm) [59], when compared with other green-emitting centres such as Eu^{2+} ($^4F_6{}^5D_1 \rightarrow {}^4F_7$) or Ce^{3+} ($^4F_6{}^5D_1 \rightarrow {}^4F_1$) incorporated in inorganic hosts, in particular, $BaSi_2O_5$:Eu^{2+},Pr^{3+} (~514 nm, FWHM ~150 nm) [60], and $Ca_{1.4}Al_{2.8}Si_{9.2}N_{16}$:$Ce^{3+}$,$Li^+$ (centre at 525 nm, FWHM ~135 nm) [61].

The fact that the energy, full-width-at-half maximum (FWHM) and number of Stark components is independent of the concentration and excitation wavelength (Fig. S6), points out that the Tb^{3+} ions occupy, in average, the same unique local environment in all the materials and, thus, that a single Tb^{3+} complex was formed in-situ. Concerning the local environment, we notice that TGA data confirmed that there is no coordination water to the Tb^{3+} ions (Fig. S5). Accordingly, the in-situ synthesis of the Tb^{3+} complex both blocks the polymeric stacking

interaction nature of multi-carboxylates and prevents the direct coordination of water molecules to Tb^{3+} ions.

The luminescence decay curves of 10TbSal@dU6, 20TbSal@dU6, and 30TbSal@dU6 are shown in Fig. S7, all monitored at 543 nm ($^5D_4 \rightarrow {}^7F_5$ of Tb^{3+} transition) at room temperature. All curves are fitted by a single exponential function yielding lifetime values of $1.2 \pm 0.1 \times 10^{-3}$ s (10TbSal@dU6) and $1.4 \pm 0.1 \times 10^{-3}$ s (20TbSal@dU6 and 30TbSal@dU6). The single exponential decay and the similarity among all the values are additional arguments towards the formation of an analogous single complex, independently of the Tb^{3+} concentration. In addition, the absolute quantum yield values are also presented in Fig. 4, in which the 30TbSal@dU6 displays the highest value, 0.565±0.057 under excitation of 360 nm. The corresponding values of 10TbSal@dU6 and 20TbSal@dU6 are 0.394±0.039 (340 nm) and 0.419±0.042 (350 nm), respectively. The increase of the quantum yield with the concentration increase may account for the contribution of the hybrid excited states. Theoretical calculations demonstrated that ligand-to-Ln^{3+} energy transfer rates are one order of magnitude larger than the values estimated for direct hybrid-to-Ln^{3+} energy transfer [62], and, then, the dominant intramolecular energy transfer pathway is hybrid-to-ligand-to-$^5D_4$, for excitation in the dU(600) singlet excited states. We notice that, as more ions are incorporated, a larger number of ligands are closer to the hybrids' excited states and thus enabling efficient energy transfer which contributes to enhancing the radiative transition probability. At lower concentrations, despite absorption occurs, less energy is transferred with the consequent decrease of the emission quantum yield.

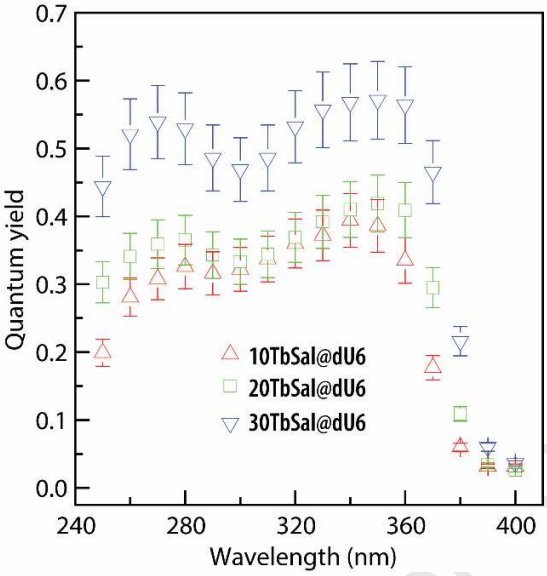

Fig. 4. Absolute quantum yields of 10TbSal@dU6, 20TbSal@dU6, and 30TbSal@dU6 based on excitation wavelength.

To unveil the potential of the hybrids to be used as UV-down shifting layers in NUV-LEDs, the photostability under NUV excitation was evaluated. Under continuous excitation (365 nm), the emission of 30TbSal@dU6 is nearly stable in the initial 15 h, revealing a decrease (~20%) in the next 13 h, Fig. 5. Aiming at comparing it with other green-emitting phosphors, we note that photostability depends on the excitation source features (energy and optical power density) and aspects related to the phosphors, namely on the physical (absorption coefficient, thickness, temperature) and chemical (concentration) properties (Table S3). Thus, an accurate comparison between data must clarify those aspects. Fig. 5 shows the normalized photostability curves of green-emitting down-shifting materials under excitation in the near-UV (365 and 370 nm) by LEDs or lamps [63–70]. Among near-UV-excited materials, only $CsPbBr_3$ nanocrystals prepared at high-temperature values (180 °C) [64] reveal better stability compared with that of 30TbSal@dU6. We also highlight that the 30TbSal@dU6 prepared in-situ using carboxylate

ligands, shows improved photostability compared to that of the $(Tb(3Cl\text{-}acac)_3(H_2O)_2$ (acac=acetylacetonate) [67] β-diketonate complex, in agreement with the reported active role of the polymeric nature from the former ligands.

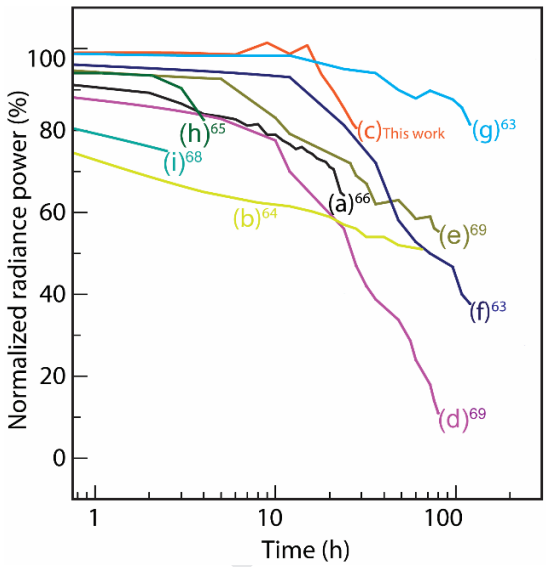

Fig. 5. Photostabilities of selected green-emitting LEDs and phosphors (Table S3). a) $Tb(3Cl\text{-}acac)_3(H_2O)_2$ [67]; b) Silica monolith doped with CdSe/CdS/ZnS quantum dots [65]; c) 30TbSal@dU6; d) Hierarchical CaF_2 nanosphere loading $CsPbBr_3$ perovskite quantum dots [70]; e) $CsPbBr_3$ perovskite quantum dots [70]; f) $CsPbBr_3$ nanocrystals [64]; g) Mesoporous silica incorporated with $CsPbBr_3$ nanocrystals [64]; h) $(pba\text{-}allyl)_2Ir(pic)@SiO_2$ (HPba= 4-(2-pyridyl)benzaldehyde and pic= picolinic acid) [66]; i) Carbon dots [69].

From the above data, we selected 30TbSal@dU6 to fabricate a green-emitting LED (Fig. 1). As a figure of merit, the optimised prototype based on 30TbSal@dU6 reveals a maximum LE of 21.5 lm/W (4.4×10^{-2} A of driving current, and 3.2 V of applied voltage) and yellowish-green emission with CIE color coordinates of (0.329, 0.606), Table S4. This LE value is the best values reported for analogous prototypes formed by a NUV-LED (365±5 nm) coated with a green-

emitting phosphor prepared either under mild synthetic conditions (<100 °C) based on Tb^{3+} ions or at high temperature from solid-state reaction for Eu^{2+} ions [36,67,71,72].

4. Conclusions

In this work, organic–inorganic di-ureasils containing a Tb^{3+} complex with the organic ligand HSal were synthesized via an in-situ sol-gel process. This in-situ synthesis was done at low temperatures ensuring energy saving and providing an alternative way to incorporate Ln^{3+}-based complexes into polymeric and hybrid matrixes (such as di-ureasils), which overcomes the poor solubility problems of Ln^{3+} complexes that are hardly dissolved and/or decompose during the sol–gel process. We demonstrated the in-situ formation of the Tb^{3+}-complex within the di-ureasil host due to the deprotonation of the carboxyl groups and the Tb^{3+} coordination with ligand anions yielding transparent coatings. The luminescent di-ureasils show bright green emission with a maximum quantum yield of 0.565±0.057 under near-UV excitation up to 365 nm, enabling the fabrication of a green-emitting prototype based on a near-UV GaN-based chip coated with the Tb^{3+}-based di-ureasil layer. The attained narrow-band green emission displays color stability, and relatively high LE (21.5 lm/W) pointing out that carboxylate-based complexes prepared in-situ using energy-saving synthesis are promising future for commercial green-emitting LED applications including solid-state lighting and backlight for flexible displays.

Acknowledgments

This work was financially supported by the project WINLEDS-POCI-01-0145-FEDER-030351 and developed within the scope of the project CICECO-Aveiro Institute of Materials, FCT Ref. UID/CTM/50011/2019, financed by national funds through the

FCT/MCTES. This work was also supported by the China Scholarship Council, grant: 201707920002 (2017–2020). AGBJ is particularly grateful to the São Paulo research foundation (FAPESP) (Grant No. 2015/10394-1, 2016/20421-9, and 2017/21995-1).

References

[1] W.D. Nordhaus, Do real-output and real-wage measures capture reality? The history of lighting suggests not, The economics of new goods, University of Chicago Press, 1996, 27–70.

[2] A. De Almeida, B. Santos, B. Paolo, M. Quicheron, Solid state lighting review - Potential and challenges in Europe, Renew. Sust. Energ. Rev. 34 (2014) 30–48.

[3] P.M. Pattison, J.Y. Tsao, G.C. Brainard, B. Bugbee, LEDs for photons, physiology and food, Nature 563 (7732) (2018) 493–500.

[4] S. Pimputkar, J.S. Speck, S.P. DenBaars, S. Nakamura, Prospects for LED lighting, Nat. Photonics 3(4) (2009) 179–181.

[5] M.S. Rea, Biophotonics: Circadian photonics, Nat. Photonics 5 (5) (2011) 271–272.

[6] M. Zhao, H.X. Liao, M.S. Molokeev, Y.Y. Zhou, Q.Y. Zhang, Q.L. Liu and Z.G. Xia, Emerging ultra-narrow-band cyan-emitting phosphor for white LEDs with enhanced color rendition, Light: Sci. Appl. 8 (2019) 38

[7] M. Rolles, B. Hyot, P. Miska, New architecture of $ZnGeN_2/In_{0.16}Ga_{0.84}N$ type-II quantum well-based green emitting LED, Phys. Status Solidi (RRL) 12 (8) (2018) 1800173.

[8] T.A. LeGates, D.C. Fernandez, S. Hattar, Light as a central modulator of circadian rhythms, sleep and affect, Nat. Rev. Neurosci. 15 (7) (2014) 443–454.

[9] P. Pust, P.J. Schmidt, W. Schnick, A revolution in lighting, Nat. Mater. 14 (5) (2015) 454–458.

[10] P.F. Smet, A.B. Parmentier, D. Poelman, Selecting conversion phosphors for white light-emitting diodes, J. Electrochem. Soc. 158 (6) (2011) R37–R54.

[11] N. Sabbatini, M. Guardigli, J.M. Lehn, Luminescent lanthanide complexes as photochemical supramolecular devices, Coord. Chem. Rev. 123 (1-2) (1993) 201–228.

[12] J.C.G. Bunzli, On the design of highly luminescent lanthanide complexes, Coord. Chem. Rev. 293 (2015) 19–47.

[13] M.O. Barsukova, S.A. Sapchenko, D.N. Dybtsev, V.P. Fedin, Scandium-organic frameworks: progress and prospects, Russ. Chem. Rev. 87 (11) (2018) 1139–1167.

[14] A. de Bettencourt-Dias, S. Viswanathan, Nitro-functionalization and luminescence quantum yield of Eu(III) and Tb(III) benzoic acid complexes, Dalton Trans. (34) (2006) 4093–4103.

[15] T. Fiedler, M. Hilder, P.C. Junk, U.H. Kynast, M.M. Lezhnina, M. Warzala, Synthesis, structural and spectroscopic studies on the lanthanoid p-aminobenzoates and derived optically functional polyurethane composites, Eur. J. Inorg. Chem. (2) (2007) 291–301.

[16] V. Tsaryuk, K. Zhuravlev, V. Zolin, P. Gawryszewska, J. Legendziewicz, V. Kudryashova, I. Pekareva, Regulation of excitation and luminescence efficiencies of europium and terbium benzoates and 8-oxyquinolinates by modification of ligands, J. Photochem. Photobio. A 177 (2-3) (2006) 314–323.

[17] M. Hilder, P.C. Junk, U.H. Kynast, M.M. Lezhnina, Spectroscopic properties of lanthanoid benzene carboxylates in the solid state: Part 1, J. Photochem. Photobio. A 202 (1) (2009) 10–20.

[18] A.R. Ramya, M.L.P. Reddy, A.H. Cowley, K.V. Vasudevan, Synthesis, crystal structure, and photoluminescence of homodinuclear lanthanide 4-(dibenzylamino)benzoate complexes, Inorg. Chem. 49 (5) (2010) 2407–2415.

[19] W. Yuan, Y.M. Cui, R.J. Shi, D.L. Tao, Y.Z. Wang, W.B. Zhang, J.T. Chen, L. Sun, S.X. Liu, Y.Z. Xu, Study on fluorescence properties of rare earth complexes influenced by steric effect, J. Rare Earth 29 (11) (2011) 1013–1017.

[20] M. Hilder, M. Lezhnina, M.L. Cole, C.M. Forsyth, P.C. Junk, U.H. Kynast, Spectroscopic properties of lanthanoid benzene carboxylates in the solid state: Part 2. Polar substituted benzoates, J. Photochem. Photobio. A 217 (1) (2011) 76–86.

[21] Y.W. Wang, Y.L. Zhang, W. Dou, A.J. Zhang, W.W. Qin, W.S. Liu, Synthesis, radii dependent self-assembly crystal structures and luminescent properties of rare earth (III) complexes with a tripodal salicylic derivative, Dalton Trans. 39 (38) (2010) 9013–9021.

[22] C.H. Zeng, F.L. Zhao, Y.Y. Yang, M.Y. Xie, X.M. Ding, D.J. Hou, S.W. Ng, Unusual method for phenolic hydroxyl bridged lanthanide CPs: Syntheses, characterization, one and two photon luminescence, Dalton Trans. 42 (6) (2013) 2052–2061.

[23] K.P. Zhuravlev, V.I. Tsaryuk, A.V. Vologzhanina, P.P. Gawryszewska, V.A. Kudryashova, Z.S. Klemenkova, Crystal Structures of New Lanthanide Hydroxybenzoates and Different Roles of LMCT State in the Excitation Energy Transfer to Eu^{3+} Ions, Chemistryselect 1 (13) (2016) 3428–3437.

[24] C.Q. Shen, T.L. Yan, Y.T. Wang, Z.J. Ye, C.J. Xu, W.J. Zhou, Synthesis, structure and luminescence properties of binary and ternary complexes of lanthanide (Eu^{3+}, Sm^{3+} and Tb^{3+}) with salicylic acid and 1,10-phenanthroline, J. Lumin. 184 (2017) 48–54.

[25] A. Ouchi, Y. Suzuki, Y. Ohki, Y. Koizumi, Structure of rare-earth carboxylates in dimeric and polymeric forms, Coord. Chem. Rev. 92 (1988) 29–43.

[26] T.R. Wang, H.R. Li, A simple and green strategy for preparing luminescent Tb^{3+} complex-based nanocomposite with stable luminescence in water, Mater. Res. Bull. 93 (2017) 28–34.

[27] X.M. Guo, H.D. Guo, L.S. Fu, H.J. Zhang, R.P. Deng, L.N. Sun, J. Feng, S. Dang, Novel hybrid periodic mesoporous organosilica material grafting with Tb complex: Synthesis, characterization and photoluminescence property, Micropor. Mesopor. Mater. 119 (1-3) (2009) 252–258.

[28] Q.M. Wang, B. Yan, Terbium/zinc luminescent hybrid siloxane-oxide materials bridged by novel ureasils linkages, J. Organomet. Chem. 691 (4) (2006) 545–550.

[29] L.S. Fu, Q.G. Meng, H.J. Zhang, S.B. Wang, K.Y. Yang, J.Z. Ni, In situ synthesis of terbium-benzoic acid complex in sol-gel derived silica by a two-step sol-gel method, J. Phys. Chem. Solids 61 (11) (2000) 1877–1881.

[30] X.P. Fan, X.H. Lv, S.B. Li, F. Wang, M.Q. Wang, The *in-situ* synthesis process and luminescence behavior of a *p*-hydroxybenzoic acid-terbium complex in sol-gel derived host materials, J. Mater. Chem. 12 (12) (2002) 3560–3564.

[31] G. Kaur, Y. Dwivedi, S.B. Rai, Gd^{3+} Sensitized Enhanced Green Luminescence in Gd:Tb$(Sal)_3$Phen Complex in PVA, J. Fluoresc. 21 (1) (2011) 423–432.

[32] T.H. Tran, M.M. Lezhnina, U. Kynast, Efficient green emission from transparent Tb^{3+}-silicone hybrid materials, J. Mater. Chem. 21 (34) (2011) 12819–12823.

[33] C.P. Montgomery, D. Parker, L. Lamarque, Effective and efficient sensitisation of terbium luminescence at 355 nm with cell permeable pyrazoyl-1-azaxanthone macrocyclic complexes, Chem. Commun. (37) (2007) 3841–3843.

[34] L. Benisvy, P. Gamez, W.T. Fu, H. Kooijman, A.L. Spek, A. Meijerink, J. Reedijk, Efficient near-UV photosensitization of the Tb(III) green luminescence by use of 2-hydroxyisophthalate ligands, Dalton Trans. (24) (2008) 3147–3149.

[35] K. Manseki, S. Yanagida, Effective and efficient photoluminescence of salicylate-ligating terbium(III) clusters stabilized by multiple phenyl-phenyl interactions, Chem. Commun. (12) (2007) 1242–1244.
[36] N.Q. Sun, L.P. Li, Y.M. Yang, A.Q. Zhang, H.S. Jia, X.G. Liu, B.S. Xu, Synthesis, characteristics and luminescent properties of a new Tb(III) ternary complex applied in near UV-based LED, Opt. Mater. 49 (2015) 39–45.
[37] V. De Bermudez, R.A.S. Ferreira, L.D. Carlos, C. Molina, K. Dahmouche, S.J.L. Ribeiro, Coordination of Eu^{3+} ions in siliceous nanohybrids containing short polyether chains and bridging urea cross-links, J. Phys. Chem. B 105 (17) (2001) 3378–3386.
[38] V. De Bermudez, L.D. Carlos, L. Alcacer, Sol-gel derived urea cross-linked organically modified silicates. 1. Room temperature mid-infrared spectra, Chem. Mater. 11 (3) (1999) 569–580.
[39] Y.T. Yang, S.Y. Zhang, Study of lanthanide complexes with salicylic acid by photoacoustic and fluorescence spectroscopy, Spectrochim. Acta A 60 (8-9) (2004) 2065–2069.
[40] L.S. Fu, R.A.S. Ferreira, M. Fernandes, S.C. Nunes, V. De Bermudez, G. Hungerford, J. Rocha, L.D. Carlos, Photoluminescence and quantum yields of organic/inorganic hybrids prepared through formic solvolysis, Opt. Mater. 30 (7) (2008) 1058–1064.
[41] B.E. Warren, X-Ray Studies of Glass Structure, Am. Ceram. Soc. Bull. 48 (9) (1969) 872.
[42] M. Fang, L.S. Fu, S.F.H. Correia, R.A.S. Ferreira, L.D. Carlos, Highly efficient luminescent polycarboxylate lanthanide complexes incorporated into di-ureasils by an in-situ sol–gel process, Polymers 10 (4) (2018) 434.
[43] K. Dahmauche, L.D. Carlos, V. De Bermudez, R.A.S. Ferreira, C.V. Santilli, A.F. Craievich, Structural modelling of Eu^{3+}-based siloxane-poly(oxyethylene) nanohybrids, J. Mater. Chem. 11 (12) (2001) 3249–3257.
[44] P.P. Lima, F.A.A. Paz, R.A.S. Ferreira, V. De Bermudez, L.D. Carlos, Ligand-assisted rational design and supramolecular tectonics toward highly luminescent Eu^{3+}-containing organic-inorganic hybrids, Chem. Mater. 21 (21) (2009) 5099–5111.
[45] L.S. Fu, R.A.S. Ferreira, N.J.O. Silva, J.A. Fernandes, P. Ribeiro-Claro, I.S. Goncalves, V. De Bermudez, L.D. Carlos, Structure–photoluminescence relationship in Eu(III) β-diketonate-based organic–inorganic hybrids. Influence of the synthesis method: carboxylic acid solvolysis versus conventional hydrolysis, J. Mater. Chem. 15 (30) (2005) 3117–3125.
[46] X.X. Li, Z.Q. Wei, S.T. Yue, N. Wang, H.H. Mo, Y.L. Liu, A new lanthanide coordination polymer with 4,4'-oxybis(benzoic acid) ligand: hydrothermal synthesis, crystal structure and photoluminescence, J. Chem. Crystallogr. 41 (5) (2011) 757–761.
[47] S. Kawaguchi, T. Kitano, K. Ito, Dissociation behavior of poly(fumaric acid) and poly(maleic acid). 3. infrared and ultraviolet spectroscopy, Macromolecules 25 (4) (1992) 1294–1299.
[48] X.W. Yang, W.J. Sun, C.Y. Ke, H.G. Zhang, X.Y. Wang, S.L. Gao, Thermochemical properties of rare earth complexes with salicylic acid, Thermochim. Acta 463 (1-2) (2007) 60–64.
[49] J.P. Huang, C.M. Li, L.L. Tao, H.L. Zhu, G. Hu, Synthesis, characterization and heterogeneous base catalysis of amino functionalized lanthanide metal-organic frameworks, J. Mol. Struct. 1146 (2017) 853–860.
[50] M.C. Yin, C.C. Ai, L.J. Yuan, C.W. Wang, J.T. Sun, Synthesis, structure and luminescent property of a binuclear terbium complex $[Tb_2(Hsal)_8(H_2O)_2][(Hphen)_2]\cdot 2H_2O$, J. Mol. Struct. 691 (1-3) (2004) 33–37.

[51] M. Fang, L.S. Fu, R.A.S. Ferreira, L.D. Carlos, White-light emitting di-ureasil hybrids, Materials 11 (11) (2018) 2246.

[52] A. Bastos, B. McKenna, M. Lima, P.S. Andre, L.D. Carlos, R.C. Evans, R.A.S. Ferreira, Flexible optical amplifier for visible-light communications based on organic-inorganic hybrids, ACS Omega 3 (10) (2018) 13772–13781.

[53] G. Kaur, S.B. Rai, Luminescence properties of Sm, $Tb(Sal)_3Phen$ complex in polyvinyl alcohol: an approach for white-light emission, J. Phys. D Appl. Phys. 44 (42) (2011) 425306.

[54] B. Yan, B. Zhou, Photophysical properties of dysprosium complexes with aromatic carboxylic acids by molecular spectroscopy, J. Photochem. Photobio. A 171 (2) (2005) 181–186.

[55] W.T. Carnall, P.R. Fields, K. Rajnak, Spectral intensities of trivalent lanthanides and actinides in solution .2. Pm^{3+}, Sm^{3+}, Eu^{3+}, Gd^{3+}, Tb^{3+}, Dy^{3+} and Ho^{3+}, J. Chem. Phys. 49 (10) (1968) 4412–4423.

[56] F.J. Steemers, W. Verboom, D.N. Reinhoudt, E.B. Vandertol, J.W. Verhoeven, New Sensitizer-modified calix[4]arenes enabling near-uv excitation of complexed luminescent lanthanide ions, J. Am. Chem. Soc. 117 (37) (1995) 9408–9414.

[57] T.R. Wang, P. Li, H.R. Li, Color-tunable luminescence of organoclay-based hybrid materials showing potential applications in white LED and thermosensors, ACS Appl. Mater. Interfaces 6 (15) (2014) 12915–12921.

[58] Y.Y. Zhao, H.R. Xu, X.Y. Zhang, G.S. Zhu, D.L. Yan, Q. Ling, M.S. Chen, A.B. Yu, Optical performances of YAG:Re^{3+} (Re = Ce, Eu) phosphor films with co-doping Tb^{3+} as energy-transfer sensitizer, J. Am. Ceram. Soc. 99 (3) (2016) 756–759.

[59] D.L. Macadam, Color Science - Concepts and methods, quantitative data and formulas, 2nd Edition - G. Wyszecki, W.S. Stiles, Opt. Eng. 22 (4) (1983) S116–S117.

[60] P. Feng, Li, G., Guo, H. J, Liu, D. W., Ye, Q. F. and Wang, Y. H., Identifying a cyan ultralong persistent phosphorescence (Ba,Li) $(Si,Ge,P)_2O_5$:Eu^{2+}, Pr^{3+} via solid solution strategy, J. Phys. Chem. C 123 (5) (2019) 3102–3109.

[61] Q.S. Wu, X.C. Wang, Z.Y. Zhao, C. Wang, Y.Y. Li, A.J. Mao, Y.H. Wang, Synthesis and luminescence characteristics of nitride $Ca_{1.4}Al_{2.8}Si_{9.2}N_{16}$:$Ce^{3+}$, Li^+ for light-emitting devices and field emission displays, J. Mater. Chem. C 2 (37) (2014) 7731–7738.

[62] P.P. Lima, S.S. Nobre, R.O. Freire, S.A. Junior, R.A.S. Ferreira, U. Pischel, O.L. Malta, L.D. Carlos, Energy transfer mechanisms in organic-inorganic hybrids incorporating europium(III): A quantitative assessment by light emission spectroscopy, J. Phys. Chem. C 111 (47) (2007) 17627–17634.

[63] Y.B. Chen, K.W. Cheah, M.L. Gong, Low thermal quenching and high-efficiency Ce^{3+}, Tb^{3+}-co-doped $Ca_3Sc_2Si_3O_{12}$ green phosphor for white light-emitting diodes, J. Lumin. 131 (8) (2011) 1589–1593.

[64] X.X. Di, L.D. Shen, J.T. Jiang, M.L. He, Y.Z. Cheng, L. Zhou, X.J. Liang, W.D. Xiang, Efficient white LEDs with bright green-emitting $CsPbBr_3$ perovskite nanocrystal in mesoporous silica nanoparticles, J. Alloys Compd. 729 (2017) 526–532.

[65] S. Jun, J. Lee, E. Jang, Highly luminescent and photostable quantum dot-silica monolith and its application to light-emitting diodes, ACS Nano 7 (2) (2013) 1472–1477.

[66] O.H. Kim, S.W. Ha, J.I. Kim, J.K. Lee, Excellent photostability of phosphorescent nanoparticles and their application as a color converter in light emitting diodes, ACS Nano 4 (6) (2010) 3397–3405.

[67] M.M. Nolasco, P.M. Vaz, P.D. Vaz, R.A.S. Ferreira, P.P. Lima, L.D. Carlos, A green-emitting α-substituted β-diketonate Tb^{3+} phosphor for ultraviolet LED-based solid-state, J. Coord. Chem. 67 (23-24) (2014) 4076–4089.

[68] F. Rahman, A.F. George, R. Drinkard, Short- and long-term reliability studies of broadband phosphor-converted red, green, and white light-emitting diodes, IEEE Trans. Device Mater. Reliab. 16 (1) (2016) 1–8.

[69] D.Y. Wang, W.U. Khan, Z.B. Tang, Y.H. Wang, Applicability evaluation of bright green-emitting carbon dots in the solid state for white light-emitting diodes, Chem. Asian J. 13 (3) (2018) 292–298.

[70] Y. Wei, H. Xiao, Z.X. Xie, S. Liang, S.S. Liang, X.C. Cai, S.S. Huang, A.A. Al Kheraif, H.S. Jang, Z.Y. Cheng, J. Lin, Highly luminescent lead halide perovskite quantum dots in hierarchical CaF_2 matrices with enhanced stability as phosphors for white light-emitting diodes, Adv. Opt. Mater. 6 (11) (2018) 1701343.

[71] T.W. Kuo, W.R. Liu, T.M. Chen, Emission color variation of $(Ba,Sr)_3BP_3O_{12}:Eu^{2+}$ phosphors for white light LEDs, Opt. Express 18 (3) (2010) 1888–1897.

[72] X.G. Zhang, X.X. Wang, J.Q. Huang, J.X. Shi, M.L. Gong, Near UV-based LED fabricated with $Ba_5SiO_4(F,Cl)_6:Eu^{2+}$ as blue- and green-emitting phosphor, Opt. Mater. 32 (1) (2009) 75–78.

TOC

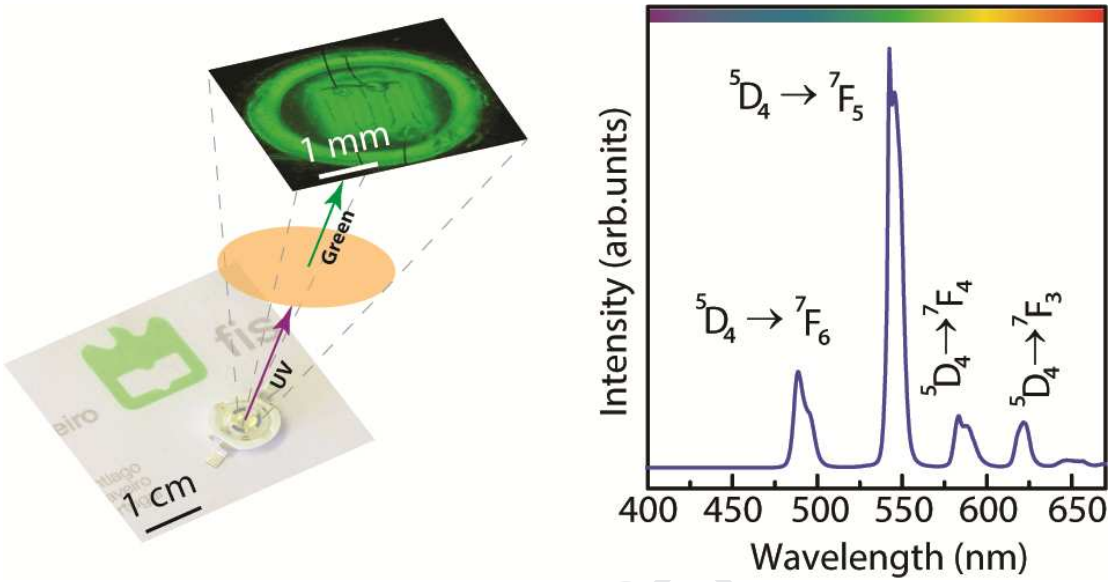

Highlights

- High doping concentration of Tb^{3+} carboxylate-based di-ureasil hybrids
- Tb^{3+}-doped di-ureasils with a high emission quantum yield (0.565±0.057)
- "π-stacking" of aromatic ligands benefits near-UV excitation
- High luminous efficacy (21.5 lm/W) of 365 nm yellowish-green LED coated with the hybrids